Published in final edited form as:
Langmuir. 2006 June 6; 22(12): 5241–5250.

Creating Advanced Multifunctional Biosensors with Surface Enzymatic Transformations

Hye Jin Lee, **Alastair W. Wark**, and **Robert M. Corn***
Department of Chemistry, University of California-Irvine, Irvine, CA 92697, USA

Abstract

This article summarizes our recent work on the coupling of surface enzyme chemistry and bioaffinity interactions on biopolymer microarrays for the creation of multiplexed biosensors with enhanced selectivity and sensitivity. The surface sensitive techniques of surface plasmon resonance imaging (SPRI) and surface plasmon fluorescence spectroscopy (SPFS) are used to detect the surface enzymatic transformations in real time. Three specific examples of novel coupled surface bioaffinity/surface enzymatic processes are demonstrated: (i) a surface enzymatic amplification method utilizing the enzyme ribonuclease H (RNase H) in conjunction with RNA microarrays that permits the ultrasensitive direct detection of genomic DNA at a concentration of 1 fM without labeling or PCR amplification, (ii) the use of RNA-DNA ligation chemistry to create renewable RNA microarrays from single stranded DNA microarrays, and (iii) the application of T7 RNA polymerase for the on-chip replication of RNA from double stranded DNA microarray elements. In addition, a simple yet powerful theoretical framework that includes the contributions of both enzyme adsorption and surface enzyme kinetics is used to quantitate surface enzyme reactivity. This model is successfully applied to SPRI and SPFS measurements of surface hydrolysis reactions of RNase H and Exonuclease III (Exo III) on oligonucleotide microarrays.

I. Introduction

The use of biopolymers attached to surfaces in a microarray format for the rapid, multiplexed identification and analysis of bioaffinity interactions has become an indispensable tool for modern biology, biochemistry and biotechnology. Surface plasmon resonance imaging (SPRI) has recently emerged as an extremely versatile method for detecting the adsorption of biomolecules onto biopolymer (e.g., DNA, RNA, peptide, protein, carbohydrate) microarrays. A schematic diagram of an SPRI apparatus is shown in Figure 1. In an SPRI experiment, the change in reflectivity from a gold thin film due to changes in the local refractive index near the surface is used to monitor the adsorption of a target bioaffinity partner from solution. The resultant SPRI difference image can be quantitatively analyzed to determine the amount of adsorption without the need for attaching a fluorophore, nanoparticle or other species to the target molecule. This means SPRI can be used to detect the adsorption of a wide variety of biomolecules including DNA, RNA, proteins, lectins and antibodies.[1-16] Figure 1b shows a set of representative SPRI difference images from various studies of bioaffinity interactions that our research group has performed over the past eight years.[6, 10-16]

While the multiplexed microarray analysis of bioaffinity interactions is a valuable research tool, even more specificity and sensitivity can be obtained by coupling the bioaffinity process to an enzymatic transformation. This coupling is often employed in solution phase biotechnological processes; for example, the coupling of DNA hybridization with the

*Correspondence should be addressed to R. M. C. (rcorn@uci.edu)

polymerase chain reaction (PCR) leads to the process of PCR amplification in genomic DNA samples.[17, 18] However, the direct incorporation of solution enzymatic methods such as PCR into a parallel microarray format is often not viable because any intermediate solution species will diffuse into neighboring array elements. Instead of using solution enzyme chemistry, it is better to utilize a surface enzyme reaction on biomolecules attached to the microarray surface. The use of surface enzyme chemistry ensures that the parallel nature of the multiplexed microarray assay remains intact.

Many new microarray methods for biosensing that incorporate both bioaffinity interactions and surface enzymatic transformations are beginning to appear in the literature. For instance, various methods for single nucleotide polymorphism (SNP) genotyping using surface polymerase extension reactions or surface ligation have been demonstrated.[19-25] We have recently developed a novel surface-based bioaffinity/enzymatic process that employs RNA microarrays and RNase H to lower the detection limit for SPRI measurements of single stranded DNA (ssDNA) to a concentration of one femtomolar.[26, 27] Figure 2 shows how this enzymatic amplification methodology works. An RNA microarray is exposed to a solution containing both a small amount of ssDNA and the enzyme RNase H. The target ssDNA first binds to a complementary RNA molecule to form an RNA-DNA heteroduplex on the surface (step 1). RNase H recognizes this surface heteroduplex and then selectively hydrolyzes the RNA, releasing both the target ssDNA and the enzyme into solution (step 2). The released ssDNA is free to hybridize with another RNA attached to the surface, and RNase H will again hydrolyze the RNA in the surface heteroduplex. This cycle of binding followed by hydrolysis will continue until eventually all of the RNA probe molecules are removed from the surface (step 3). Note that this surface RNase H amplification process differs from traditional ELISA-style sandwich enzymatic amplification methods[28] because: (i) the enzyme substrate is not in solution but instead is attached to the surface, (ii) the surface enzyme reaction releases the enzyme back into solution, and (iii) the RNase H amplification process requires the repeated binding of the target molecule to the surface.

This article describes the recent experimental and theoretical advances we have made in the coupling of surface bioaffinity processes to surface enzymatic reactions such as RNase H hydrolysis for enhanced biosensing applications. In Section II, a simple theoretical framework is presented to quantitate the reaction of an enzyme in solution with a surface immobilized substrate. This basic coupled reaction scheme forms the foundation for all of our surface enzymatic amplification and transformation processes. In Section III this model is then used to characterize the surface enzyme chemistry of RNase H and Exonuclease III; a combination of SPRI and surface plasmon fluorescence spectroscopy (SPFS) is employed to obtain a set of surface enzyme kinetic parameters. Finally, in Section IV, specific examples demonstrating several different coupled surface bioaffinity/surface enzymatic transformations on DNA and RNA microarrays are presented. These new surface processes include: (i) the RNase H amplification methodology described above for the ultrasensitive detection of genomic DNA, (ii) the application of surface ligation chemistry for the fabrication of RNA microarrays from a DNA microarray template, and (iii) a new method using RNA polymerase for the replication of multiple single stranded RNA (ssRNA) molecules from double stranded DNA (dsDNA) microarray elements.

II. Theory of Coupled Langmuir Adsorption and Surface Enzyme Kinetics

In this section we quantitatively describe the reaction of an enzyme in solution with a surface immobilized substrate. We find that the surface coverage of the enzyme-substrate intermediate is governed by an interesting combination of Langmuir adsorption kinetics and Michaelis-Menten concepts. Before introduction of the coupled equations, however, we first review how classical Langmuir kinetics affects surface bioaffinity measurements.

A. Langmuir Adsorption and Desorption Kinetics

The vast majority of surface bioaffinity measurements utilize the specific adsorption of target biomolecules (*T*) from solution onto a surface that has been chemically modified with probe biomolecules (*P*). If the target and probe interact in a simple 1:1 ratio, then in the absence of bulk transport the surface reaction can be represented in the form:

$$T+P \underset{k_d}{\overset{k_a}{\rightleftarrows}} TP \tag{1}$$

where *TP* is the surface bound target-probe complex (see also Figure 3 inset). An example of such a reaction would be the adsorption of an ssDNA 16mer target molecule onto a surface bound ssDNA 16mer probe molecule to form a surface bound dsDNA duplex (we define this process as "hybridization adsorption"). Both *P* and *TP* are surface species, and in the Langmuir approximation their surface concentrations, Γ_P and Γ_{TP}, are linked to the total concentration of surface sites (Γ_{tot}) by eq 2:

$$\Gamma_P+\Gamma_{TP}=\Gamma_{tot} \tag{2}$$

If we define θ as the fraction of occupied surface sites, $\theta = \Gamma_{TP}/\Gamma_{tot}$, then surface adsorption and desorption kinetics can be described by eq 3:

$$\frac{d\theta}{dt}=k_a(1-\theta)[T]-k_d\theta \tag{3}$$

At equilibrium, the fractional surface coverage reaches a steady state ($d\theta/dt = 0$) and this equilibrium surface coverage θ_{eq} is given by the Langmuir adsorption isotherm:

$$\theta_{eq}=\frac{K_{ads}[T]}{1+K_{ads}[T]} \tag{4}$$

where the Langmuir adsorption coefficient K_{ads} is defined as $K_{ads} = k_a/k_d$. A typical Langmuir analysis for 16mer DNA hybridization adsorption is shown in Figure 3 with a K_{ads} of about 2.0×10^7.[16,29] At a bulk concentration equal to $1/K_{ads}$, half of the surface sites are occupied (i.e., $\theta_{eq} = 0.5$). For 16mer ssDNA hybridization adsorption, this concentration value is 50 nM.

Equation 3 can also be integrated depending upon the initial conditions to determine the time dependence of the fractional surface coverage, $\theta(t)$. For the case of adsorption from a solution of concentration [*T*] onto an unoccupied surface, the time dependent fractional surface coverage is given by eq 5:

$$\theta(t)=\theta_{eq}\left(1-e^{-(k_a[T]+k_d)t}\right) \tag{5}$$

where θ_{eq} is the equilibrium value for θ at a particular bulk concentration, as given using eq 4. For the case when $\theta = 1$ at $t = 0$, the desorption rate can be described by eq 6:

$$\theta(t)=\theta_{eq}e^{-k_d t} \tag{6}$$

Equations 5 and 6 have been used frequently to analyze the adsorption of biomolecules onto surfaces, especially with SPR[30] and SPRI.[6] For the case of 16mer ssDNA hybridization adsorption, typical values are a k_a of ~1.5×10^4 $M^{-1}\cdot s^{-1}$, and a k_d of ~6×10^{-4} s^{-1} (data not shown).

An important question to ask is: "What is the lowest concentration one can measure with a surface-based biosensor?" The answer to this question depends upon the value of the Langmuir adsorption coefficient, which determines the equilibrium fractional surface coverage, θ_{eq}. For example, in the case of detecting 16mer ssDNA molecules by hybridization adsorption onto a DNA microarray, θ_{eq} is equal to 2×10^{-8} for a target concentration of one femtomolar. This means that the biosensing technique must be able to see two molecules per 100 million

adsorption sites in order to detect hybridization adsorption from a 1 fM solution. For a typical probe surface coverage of 5×10^{12} molecules·cm^{-2}, this corresponds to a surface coverage of roughly 10^5 molecules·cm^{-2}, or just 3 molecules in a 50 micron array element! Normal SPRI has a sufficient sensitivity to detect hybridization adsorption from 1 nM target solutions;[4, 16, 29, 31, 32] nanoparticle enhanced SPRI can detect hybridization adsorption from 1 pM target solutions.[33] For comparison, a typical fluorescence-based assay is limited by background to a detection limit of 1 pM for DNA hybridization adsorption.[31, 34, 35] In addition, at a target concentration of 1 pM the surface signal is limited by both adsorption kinetics (eq 5) and diffusion to the surface.

B. Coupled Langmuir Adsorption and Surface Enzyme Kinetics

To solve some of the problems associated with the direct detection of surface bioaffinity events at very low target concentrations, we have implemented enzymatic surface amplification schemes such as the RNase H system described previously in the Introduction. This surface amplification scheme differs from previous surface enzymatic amplification methodologies in that the substrate of the enzyme is bound to the surface. The rate of surface enzyme reaction is a critical parameter in this amplification scheme; if the surface reaction rate is too slow as compared to other side reactions, then significant amplification will not occur.

For this reason, we have recently developed a kinetic analysis of these surface enzyme reaction rates, and have made SPRI and SPFS measurements to determine the surface catalysis rate constants. We have chosen the simplest possible model for the surface enzyme reaction, which is defined using the three processes shown in Figure 4. This reaction scheme can be written as eqs 7-9:

$$E_{(x=\infty)} \xrightarrow{k_m} E_{(x=0)} \tag{7}$$

$$S + E_{(x=0)} \underset{k_d}{\overset{k_a}{\rightleftarrows}} ES \tag{8}$$

$$ES \xrightarrow{k_{cat}} S^* + E_{(x=0)} \tag{9}$$

where $E_{(x=\infty)}$ and $E_{(x=0)}$ are the bulk and surface enzyme concentrations respectively, S is the RNA-DNA surface bound substrate (the RNA-DNA heteroduplex), ES is the surface enzyme-substrate complex (the RNase H-heteroduplex complex), S^* is the surface product (ssDNA), and k_{cat} is the surface reaction rate for the enzyme complex. For the case of SPRI in microfluidic channels, the diffusion is governed by a steady state mass transport coefficient (k_m) that can also be written as D/δ where D is the diffusion coefficient for the enzyme and δ is the steady state diffusion layer thickness.[36, 37] This simplified scheme also assumes that there are only simple, non-interacting 1:1 substrate-enzyme surface complexes, and there is no adsorption of the enzyme E onto inactive surface sites.

The kinetics for this reaction scheme are governed by eqs 10-12:

$$\theta_S + \theta_{ES} + \theta_{S^*} = 1 \tag{10}$$

$$\frac{d\theta_{ES}}{dt} = \frac{k_a [E]\left(1 - \theta_{ES} - \theta_{S^*}\right) - (k_d + k_{cat})\theta_{ES}}{1 + \beta\left(1 - \theta_{ES} - \theta_{S^*}\right)} \tag{11}$$

$$\frac{d\theta_{S^*}}{dt} = k_{cat}\theta_{ES} \tag{12}$$

where the fractional surface coverages for the three surface species *S, ES* and *S** are denoted as $\theta_x=\Gamma_x/\Gamma_{tot}$ where x = *S, ES* or *S**, [*E*] is the bulk enzyme concentration and β is a dimensionless diffusion parameter[36, 37] defined by eq 13:

$$\beta=\frac{k_a\Gamma_{tot}}{k_m}=\frac{k_a\Gamma_{tot}\delta}{D} \tag{13}$$

By solving eqs 11 and 12 using simple Euler integration methods with the initial conditions $\theta_S = 1$ and $\theta_{ES} = \theta_{S*} = 0$ at time $t = 0$, the time-dependent surface coverages $\theta_{ES}(t)$, $\theta_S(t)$, and $\theta_{S*}(t)$ can be individually profiled over the course of the enzymatic reaction.

Figure 5 shows an example of a kinetic simulation for a surface enzyme reaction where k_{cat} and $k_a[E]$ are arbitrarily set equal to 0.1 s^{-1}, k_d is fixed at 0.01 s^{-1}, with $\beta = 0$ in Fig. 5a and $\beta = 10$ in Fig. 5b. As seen in this figure, θ_S drops monotonically to zero while θ_{S*} increases to one as the reaction progresses with the time-dependent changes in surface coverage of each reactant species considerably slower when $\beta \neq 0$. The kinetic profile of $\theta_{ES}(t)$ changes significantly during the reaction, initially rising to a maximum value followed by a slower decrease to zero. Consequently, a steady state approximation for the surface enzyme concentration ($d\theta_{ES}/dt = 0$) is NOT valid in this case and can only be applied when the surface reaction is very slow ($k_{cat} << k_a[E]$). The equations associated with this limiting case scenario have been derived and discussed elsewhere.[38]

Although θ_{ES} is not constant during the surface enzyme reaction, we found previously that, in all cases, the fractional surface coverage of *ES* on the *unreacted* surface sites does reach a steady-state value.[38] This fractional surface coverage is defined as λ_{ES} and is given by eq 14:

$$\lambda_{ES}=\frac{\theta_{ES}}{\theta_{ES}+\theta_S}=\frac{\theta_{ES}}{1-\theta_{S*}} \tag{14}$$

The dependence of the steady-state value of λ_{ES} on $k_a[E]$, k_d, and k_{cat} can also be expressed analytically using the following quadratic equation:

$$\lambda_{ES}=-\frac{k_a[E]}{k_{cat}\lambda_{ES}}+\frac{(k_a[E]+k_d+k_{cat})}{k_{cat}} \tag{15}$$

Figure 6 plots the variation in λ_{ES} obtained using eq 15 as a function of log ($k_{cat}/k_a[E]$) with the same fixed values of $k_a[E] = 0.1$ s^{-1} and $k_d = 0.01$ s^{-1}. Note that when $k_{cat} << k_a[E]$, λ_{ES} approaches the Langmuir equilibrium surface coverage of 0.909 obtained using eq 4. Also, when k_{cat} is equal to $k_a[E]$, a steady state value of $\lambda_{ES} = 0.728$ is obtained. This value is the same as that observed previously in Figure 5 for both $\beta = 0$ and $\beta \neq 0$. Finally, if k_{cat} is much larger than $k_a[E]$, then λ_{ES} approaches zero and the enzyme reaction velocity is solely limited by the enzyme adsorption kinetics.

III. Quantitative Analysis of Surface RNase H and Exo III Reactions

The kinetic model described above has been applied to the quantitative analysis of the catalytic behavior of RNase H and Exo III on surface-immobilized double-stranded oligonucleotide substrates. Figure 7a shows a real-time SPRI kinetic curve acquired for the Exo III hydrolysis of dsDNA microarray elements at a temperature of 20°C. In this figure, the value of Δ%R initially rises rapidly before gradually decaying to a negative steady-state value. This biphasic signal occurs because all surface adsorption and desorption binding events contribute to the measured SPRI response; in this case, changes in the SPRI signal arise from an increase due to enzyme adsorption ($\theta_{ES}(t)$), and a decrease due to both heteroduplex hydrolysis ($\theta_{S*}(t)$) and release of enzyme back into solution. The observation of a biphasic signal suggests that the rate of Exo III adsorption ($k_a[E]$) must be equal to or greater than the rate of duplex cleavage (k_{cat}) during the initial reaction stages. Table 1 summarizes the values of k_a, k_d, and k_{cat}

obtained using our kinetic model to simultaneously fit a series of kinetic curves acquired over a range of Exo III concentrations. The data in Figure 7a is for an enzyme concentration of 320 nM; indeed, at this concentration we find that $k_a[E]$ is about eight times greater than k_{cat}. Furthermore, the values of θ_{eq} and λ_{ES} obtained using eqs 4 and 15 are similar in size (0.56 and 0.54, respectively).

Compared with the Exo III reaction, the shape of the real-time SPRI curve for the RNase H hydrolysis of RNA-DNA heteroduplex array elements in Figure 7b is qualitatively very different. At no point during the RNase H reaction is a net increase in SPRI signal observed. This suggests that $\theta_{ES}(t)$ has a negligible contribution to the measured SPRI response. The values of k_a, k_d and k_{cat} obtained from a kinetic analysis of the RNase H reaction are summarized in Table 1. The measured k_{cat} value of 1.0 s^{-1} is significantly larger than k_{cat} for the Exo III reaction, and at an RNase H concentration of 1 nM (corresponding to the data in Figure 7b), $k_{cat}/k_a[E]$ is about 300 with both λ_{ES} ($\sim 10^{-3}$) and θ_{eq} ($\sim 10^{-2}$) very small. This explains why an initial increase in SPRI signal is observed for Exo III but not for RNase H; once adsorbed, RNase H reacts very quickly and is immediately released from the surface.

When using our kinetic model to analyze the real-time SPRI response, it is necessary to make an assumption on the relative contributions of enzyme adsorption and duplex hydrolysis to the measured SPRI signal. To remove this ambiguity, it is important to obtain an independent set of in-situ surface coverage measurements. This can be achieved by fluorescently labeling one of the reaction species and applying the technique of SPFS to monitor the enzyme reaction. The combined use of SPR and SPFS measurements has previously been demonstrated by Knoll *et al.* to investigate a variety of surface biochemical interactions,[39-42] and Kim *et al.* were able to characterize protease activity on a labeled monolayer of BSA.[43]

To obtain a complete characterization of the RNase H surface reaction, time-resolved SPFS measurements were used to monitor the removal of surface bound fluorescently labeled RNA molecules by RNase H hydrolysis.[44] A schematic diagram of the SPFS apparatus is shown in Figure 8. The SPFS signal is a direct measure of $\theta_S(t)$, and can be analyzed using eqs 10-12 in an approach similar to SPRI data analysis. The solid lines in Figure 9 represent the best fit to four SPFS curves obtained at various enzyme concentrations. The k_a, k_d and k_{cat} values that generated the best fit are listed in Table 1 and are almost identical to the values obtained from the SPRI data, implying that fluorescence labeling of RNA does not significantly affect k_{cat}. Only the value of β was significantly different with $\beta = 650$ for SPFS, compared to a value of 180 for SPRI. This is due to differences in the microfluidic designs used for continuous sample delivery in the SPFS and SPRI measurements. In contrast, for Exo III no significant contribution for diffusion ($\beta = 0$) to the measured SPRI response was observed due to the much lower rates of enzyme adsorption and catalysis.

IV. Examples of Coupling Bioaffinity Interactions to Surface Enzymatic Transformations

A. RNase H Amplified Detection of DNA

As a first example of how to use surface enzymatic transformations to enhance our biosensing capabilities, we demonstrate the application of the RNase H surface enzyme process for DNA sensing using the amplified detection scheme described previously in Figure 2. The sensitivity of RNase H amplified measurements was determined by performing a number of experiments to detect ssDNA at various concentrations. Figure 10a shows an SPRI difference image obtained upon the hybridization adsorption of a target 24mer ssDNA (100 nM) onto ssRNA microarray elements in a two-component array (the second type of array element was a 20mer ssDNA negative control). A 1.7% increase in reflectivity from the RNA probe array elements

was observed upon hybridization adsorption (Fig. 10c). If the same microarray was instead exposed to a solution containing 100 pM ssDNA and 16 nM of RNase H, a significant (-3.4 Δ %R) loss in SPRI signal was observed as shown in Figures 10b and 10c. Note that the change in Δ%R is significantly amplified in the presence of RNase H, despite a 1000-fold reduction in ssDNA concentration. The -3.4% signal loss corresponds to the removal of all ssRNA from the surface. A similar *final* change in Δ%R is observed at other ssDNA and RNase H concentrations; however, the reaction timescales increase as the target concentration is lowered.

The dependence of the initial rate of SPRI signal loss on the ssDNA target concentration during RNase H amplified SPRI detection is shown in Figure 11. The shape of the concentration dependence curve is similar to the plot of the fractional surface coverage versus concentration for an adsorbing species, θ, predicted by the Langmuir isotherm. A fit of the data (solid line) using eq 4 yields an adsorption coefficient (K_{ads}) of 6.6×10^7 M^{-1}. This number is in good agreement with previously reported literature values for oligonucleotide hybridization adsorption.[16, 29] This data suggests that the initial reaction rate is related to the fractional surface coverage of RNA-DNA heteroduplexes via the Langmuir isotherm and can be used as a measure of target ssDNA concentration.

The sensitivity of RNase H amplified SPRI is sufficient to detect both short (16-24mers) oligonucleotides at femtomolar concentrations and also longer genomic DNA fragments *without* PCR amplification. Figure 12a shows an SPR difference image acquired after a two hour exposure of a microarray composed of three non-interacting RNA components (R1, R2 and R3) to RNase H and 1 fM target 20mer DNA which is complementary to R2. A decrease in percent reflectivity of -0.7% was observed due to the removal of R2 probes from the surface. The R1 and R3 array elements were unaffected by the enzyme. Two of the RNA probe sequences in the array (R1 and R2) were specifically designed to bind to the TSPY gene on the Y chromosome.[26] Figure 12b shows the result of an experiment exposing the three component RNA microarray to genomic DNA. The concentration of the TSPY gene sequences in the commercially available male genomic DNA was estimated to be 7 fM.[26] When the array was exposed to the genomic DNA for about 4 hours, a significant decrease in SPRI signal (-0.7%) was observed for R1 and R2 while no SPRI signal loss was observed in either R3 or background. As a control, enzymatically amplified SPRI experiments were performed on female genomic DNA under the same conditions; no decrease in SPRI signal from any of the array elements was observed. These experiments demonstrate that RNase H amplified SPRI is sufficiently sensitive to directly detect specific DNA sequences from genomic samples without any PCR amplification, labeling or other sample treatments.

B. Creating RNA Microarrays using RNA-DNA Surface Ligation Chemistry

A second example of coupling surface bioaffinity interactions and surface enzyme chemistry is the use of ligation chemistry to create RNA microarrays from DNA microarrays. The ability to fabricate stable and active ssRNA microarrays is essential not only for a successful RNase H amplified SPRI measurement, but also will be useful for the study of RNA-RNA, RNA-DNA, RNA-protein and other bioaffinity interactions. At present, the number of reports in the literature on the fabrication of ssRNA microarrays[26, 27, 45, 46] is very small compared to the wealth of information available on ssDNA microarrays.[47-50] This is mostly due to the difficulty in tethering RNA molecules to a surface without loss of functionality. Previously, we chemically attached thiol-modified RNA to maleimide-terminated alkanethiol monolayers[26, 27] and the use of biotin-modified RNA has also been reported.[45] However, these procedures are more expensive and can lead to RNA degradation during both the modification and surface attachment procedures. An alternative approach recently developed in our group is to ligate unmodified RNA onto a DNA microarray.[51] This surface enzymatic

process can be performed in-situ immediately prior to microarray use thus reducing environmental risks, such as exposure to nucleases, which can lead to RNA hydrolysis.

A simple schematic for the fabrication of an ssRNA microarray using RNA-DNA ligation chemistry is shown in Figure 13. The enzyme T4 DNA ligase is used to form a phosphodiester bond between the juxtaposed 5′ phosphate of the surface attached ssDNA (D_A) and the 3′ hydroxyl group of unmodified RNA (R_P) in the presence of a complementary ssDNA template (D_T). On completion of the ligation reaction, the array surface is thoroughly rinsed with 8 M urea in order to denature and remove the DNA template and any T4 DNA ligase, resulting in the creation of biologically active ssRNA array elements (Fig. 13b). The SPR difference image [b-a] in Figure 13 shows a Δ%R increase of 2.2% following the ligation of 24mer RNA. A surprising yet very useful feature of this approach is that the surface ligation process can be repeated to create a new RNA microarray from the same original ssDNA microarray. This is because RNase H specifically cleaves the phosphodiester bonds in the RNA component of a RNA-DNA heteroduplex to produce 5′ phosphate and 3′ hydroxyl termini. The ligation-hydrolysis cycle was repeated up to three times using the same ssDNA microarray without any degradation in SPRI signal. The ligated RNA microarray was also successfully utilized in an RNase H amplified SPRI experiment for the detection of 1 pM DNA with the initial rate of change in Δ%R observed to be over twenty times faster than that observed using microarrays prepared with thiol-modified RNA. This superior performance is attributed to an increase in RNase H activity due to the anchor DNA sequence spacing R_P further from the gold surface.

C. Replication of ssRNA from DNA Template Microarrays

The previous two examples utilized bioaffinity processes involving ssRNA attached onto the microarray surface. In this final example, we are interested in generating multiplexed samples of ssRNA in solution for bioaffinity sensing. This array-based ssRNA synthesis will be useful for the characterization of RNA-protein, RNA-peptide and RNA-small molecule interactions.[45, 46, 52, 53] On-chip replication of RNA has several advantages: i) it reduces the risk of RNA degradation by eliminating any ex-situ handling, ii) the synthesized RNA sample is sufficiently concentrated so that weak binding interactions can be detected, and iii) if desired, on-chip collection can be used to simplify the purification of the synthesized ssRNA product.

The scheme in Figure 14 shows a method for the generation of ssRNA from a dsDNA microarray element (P1) using T7 RNA polymerase. The ssRNA is subsequently detected via hybridization adsorption onto a second array element (P2). The ssRNA can also be used in other bioaffinity measurements with protein or peptide microarrays. The P1 array element contains dsDNA formed by hybridization of a ssDNA template sequence (T) to a surface bound promoter DNA sequence (P) (Fig. 14a). The dsDNA complexes on P1 could be composed of just the T7 RNA polymerase promoter sequence, or also include additional nucleotides complementary to T. The P2 array element is designed to bind to the C region of the ssRNA strands replicated by the polymerase reaction. When the P1 array elements are exposed to T7 polymerase, the enzyme binds to the promoter region and creates ssRNA that is complementary to the template sequence (Figure 14b). Following the RNA transcription, both T7 polymerase and the ssRNA are released into the solution. T7 RNA polymerase is free to rebind repeatedly to the P1 array element, initiating the production of multiple ssRNA copies of the template. The released ssRNA is detected on the P2 array element (Figure 14c) via sequence specific hybridization adsorption of the capture sequence (C).

A two-component microarray was constructed to demonstrate the surface RNA polymerase reaction. SPRI difference images from this array during the RNA replication process are shown in Figure 14. The data in the figure confirms that we can synthesize and subsequently capture ssRNA on the microarray surface. Future work will focus on generating multiple RNA sequences simultaneously for bioaffinity sensing. For example, a microfluidic system with an

upstream surface for synthesizing multiplexed RNA sequences can be used in conjunction with a downstream protein or peptide microarray for the study of RNA-protein/RNA/aptamer bioaffinity interactions.

V. Summary and Outlook

In this article, we have highlighted the potential of surface enzyme chemistry as an invaluable surface bioengineering tool whose incorporation into novel microarray based biosensing methodologies can be an extremely effective approach for increasing both the sensitivity and specificity of multiplexed surface bioaffinity measurements. The lowering of the detection limit to 1 fM for the direct detection and identification of any desired DNA sequences including short oligonucleotides and genomic DNA with RNase H amplified SPRI is an extraordinary improvement compared to the previous nanomolar detection limit of SPRI based solely on hybridization adsorption. Fluorescence imaging has a typical detection limit of 1 pM,[31, 34, 35] therefore enzymatically amplified fluorescence measurements should have a detection limit well below 1 fM, perhaps with the ability to detect single molecular binding events.

In addition, we have demonstrated that the combination of SPRI and SPFS measurements can be used in conjunction with a simple yet powerful kinetic model to quantitatively characterize surface enzyme reactions. The quantitative characterization of surface enzyme reactions is essential because an enzyme can react orders of magnitude more slowly on a surface as compared to in solution. The kinetic model used here has only three parameters (k_a, k_d and k_{cat}), but has been successfully applied to describe both RNase H and Exo III surface hydrolysis reactions. For more complex surface enzyme transformations, we will have to develop more complicated kinetic models. Moreover, the continued use of SPRI and SPFS measurements will allow us to optimize the surface enzyme chemistry through changes in surface density, orientation and vertical spacing of the immobilized substrate.

The RNase H amplification process on RNA microarrays is only one of many possible enzymes that can be utilized on biomolecules attached to microarray surfaces. For example, we have also shown that the ligation of RNA to ssDNA microarrays can create multiplexed RNA microarrays, and the reaction of T7 RNA polymerase with surface bound dsDNA can be used to replicate multiple RNA sequences on microarrays. These two RNA fabrication processes can circumvent many of the difficulties normally associated with the handling of multiple RNA sequences in a microarray format. Other enzymes such as proteases and kinases can also be applied to process surface attached substrate molecules. All the experiments reported in this paper were performed on gold thin films for SPRI; the coupling of surface enzyme chemistry to bioaffinity interactions can occur on other surfaces (e.g., glass, silicon) and can be used in conjunction with other detection methods such as electrochemical measurements and nanoparticle and fluorescence labeling. We expect that in the future many more surface enzymatic processes will be coupled to multiplexed surface bioaffinity interactions to create highly specific and sensitive novel surface biosensors.

ACKNOWLEDGMENT

This research is funded by the National Institute of Health (2RO1 GM059622-04) and the National Science Foundation (CHE-0133151). The authors would like to thank Dr. Terry T. Goodrich for obtaining the SPR difference images shown in Figure 14.

References

1. Wolf LK, Fullenkamp DE, Georgiadis RM. J. Am. Chem. Soc 2005;127:17453–17459. [PubMed: 16332097]
2. Kanda V, Kitov P, Bundle DR, McDermott MT. Anal. Chem 2005;77:7497–7504. [PubMed: 16316154]

3. Kyo M, Usui-Aoki K, Koga H. Anal. Chem 2005;77:7115–7121. [PubMed: 16285656]
4. Okumura A, Sato Y, Kyo M, Kawaguchi H. Anal. Biochem 2005;339:328–337. [PubMed: 15797574]
5. Kyo M, Yamamoto T, Motohashi H, Kamiya T, Kuroita T, Tanaka T, Engel JD, Kawakami B, Yamamoto M. Genes to Cells 2004;9:153–164. [PubMed: 15009092]
6. Wegner GJ, Wark AW, Lee HJ, Codner E, Saeki T, Fang S, Corn RM. Anal. Chem 2004;76:5677–5684. [PubMed: 15456285]
7. Shumaker-Parry JS, Campbell CT. Anal. Chem 2004;76:907–917. [PubMed: 14961720]
8. Shumaker-Parry JS, Zareie MH, Aebersold R, Campbell CT. Anal. Chem 2004;76:918–929. [PubMed: 14961721]
9. Wilkop T, Wang Z, Cheng Q. Langmuir 2004;20:11141–11148. [PubMed: 15568869]
10. Wegner GJ, Lee HJ, Marriott G, Corn RM. Anal. Chem 2003;75:4740–4746. [PubMed: 14674449]
11. Smith EA, Thomas WD, Kiessling LL, Corn RM. J. Am. Chem. Soc 2003;125:6140–6148. [PubMed: 12785845]
12. Smith EA, Erickson MG, Ulijasz AT, Weisblum B, Corn RM. Langmuir 2003;19:1486–1492.
13. Wegner GJ, Lee HJ, Corn RM. Anal. Chem 2002;74:5161–5168. [PubMed: 12403566]
14. Smith EA, Kyo M, Kumasawa H, Nakatani K, Saito I, Corn RM. J. Am. Chem. Soc 2002;124:6810–6811. [PubMed: 12059186]
15. Lee HJ, Goodrich TT, Corn RM. Anal. Chem 2001;73:5525–5531. [PubMed: 11816583]
16. Nelson BP, Grimsrud TE, Liles MR, Goodman RM, Corn RM. Anal. Chem 2001;73:1–7. [PubMed: 11195491]
17. Gonzalez SF, Krug MJ, Nielsen ME, Santos Y, Call DR. J. Clin. Microbiol 2004;42:1414–1419. [PubMed: 15070982]
18. Sengupta S, Onodera K, Lai A, Melcher U. J. Clin. Microbiol 2003;41:4542–4550. [PubMed: 14532180]
19. Hashimoto M, Hupert ML, Murphy MC, Soper SA, Cheng Y-W, Barany F. Anal. Chem 2005;77:3243–3255. [PubMed: 15889915]
20. Hultin E, Kaller M, Ahmadian A, Lundeberg J. Nucl. Acids Res 2005;33:e48. [PubMed: 15767273]
21. Deng J, Zhang X, Manga Y, Zhang Z, Zhou Y, Liu Q, Lu H, Fu Z. Biosens. Bioelectron 2004;19:1277–1283. [PubMed: 15046760]
22. Giusto DD, King GC. Nucl. Acids Res 2003;31:e7. [PubMed: 12560510]
23. Zhong X, Reynolds R, Kidd JR, Kidd KK, Jenison R, Marlar RA, Ward DC. Proc. Natl. Acad. Sci. USA 2003;100:11559–11564. [PubMed: 12975525]
24. Broude NE, Woodward K, Cavallo R, Cantor CR, Englert D. Nucl. Acids Res 2001;29:e92. [PubMed: 11574694]
25. Gerry NP, Witowski NE, Day J, Hammer RP, Barany G, Barany F. J. Mol. Biol 1999;292:251–262. [PubMed: 10493873]
26. Goodrich TT, Lee HJ, Corn RM. J. Am. Chem. Soc 2004;126:4086–4087. [PubMed: 15053580]
27. Goodrich TT, Lee HJ, Corn RM. Anal. Chem 2004;76:6173–6178. [PubMed: 15516107]
28. Crowther, JR. ELISA: Theory and Practice. 1st ed.. 42. Humana Press Inc.; Totowa, NJ: 1995.
29. Wark AW, Lee HJ, Corn RM. Anal. Chem 2005;77:3904–3907. [PubMed: 15987090]
30. O'Shannessy DJ, Brigham-Burke M, Soneson KK, Hensley P, Brooks I. Anal. Biochem 1993;212:457–468. [PubMed: 8214588]
31. Livache T, Maillart E, Lassalle N, Mailley P, Corso B, Guedon P, Roget A, Levy Y. J. Pharm. Biomed. Anal 2003;32:687–696. [PubMed: 12899959]
32. Guedon P, Livache T, Martin F, Lesbre F, Roget A, Bidan G, Levy Y. Anal. Chem 2000;72:6003–6009. [PubMed: 11140769]
33. He L, Musick MD, Nicewarner SR, Salinas FG, Benkovic SJ, Natan MJ, Keating CD. J. Am. Chem. Soc 2000;122:9071–9077.
34. Lehr H-P, Reimann M, Brandenburg A, Sulz G, Klapproth H. Anal. Chem 2003;75:2414–2420. [PubMed: 12918985]
35. Zammatteo N, Jeanmart L, Hamels S, Courtois S, Louette P, Hevesi L, Remacle J. Anal. Biochem 2000;280:143–150. [PubMed: 10805532]

36. Bourdillon C, Demaille C, Moiroux J, Saveant J. J. Am. Chem. Soc 1999;121:2401–2408.
37. Schuck P, Minton AP. Anal. Biochem 1996;240:262–272. [PubMed: 8811920]
38. Lee HJ, Wark AW, Goodrich TT, Fang S, Corn RM. Langmuir 2005;21:4050–4057. [PubMed: 15835973]
39. Stengel G, Knoll W. Nucl. Acids Res 2005;33:e69. [PubMed: 15849312]
40. Tawa K, Knoll W. Nucl. Acids Res 2004;32:2372–2377. [PubMed: 15115799]
41. Yao D, Yu F, Kim J, Scholz J, Nielsen PE, Sinner E, Knoll W. Nucl. Acids Res 2004;32:e177. [PubMed: 15598819]
42. Yu F, Yao D, Knoll W. Anal. Chem 2003;75:2610–2617. [PubMed: 12948127]
43. Kim J-H, Roy S, Kellis JT Jr. Poulose AJ, Gast AP, Robertson CR. Langmuir 2002;18:6312–6318.
44. Fang S, Lee HJ, Wark AW, Kim HM, Corn RM. Anal. Chem 2005;77:6528–6534. [PubMed: 16223236]
45. Collett JR, Cho EJ, Lee JF, Levy M, Hood AJ, Wan C, Ellington AD. Anal. Biochem 2005;338:113–123. [PubMed: 15707941]
46. McCauley TG, Hamaguchi N, Stanton M. Anal. Biochem 2003;319:244–250. [PubMed: 12871718]
47. Levicky R, Horgan A. Trends in Biotech 2005;23:143–149.
48. Stoughton RB. Annu. Rev. Biochem 2005;74:53–82. [PubMed: 15952881]
49. Epstein JR, Biran I, Walt DR. Anal. Chim. Acta 2002;469:3–36.
50. Heller MJ. Annu. Rev. Biomed. Eng 2002;4:129–153. [PubMed: 12117754]
51. Lee HJ, Wark AW, Li Y, Corn RM. Anal. Chem 2005;77:7832–7837. [PubMed: 16316195]
52. Rusconi CP, Scardino E, Layzer J, Pitoc GA, Ortel TL, Monroe D, Sullenger BA. Nature 2002;419:90–94. [PubMed: 12214238]
53. Tasset DM, Kubik MF, Steiner W. J. Mol. Biol 1997;272:688–698. [PubMed: 9368651]

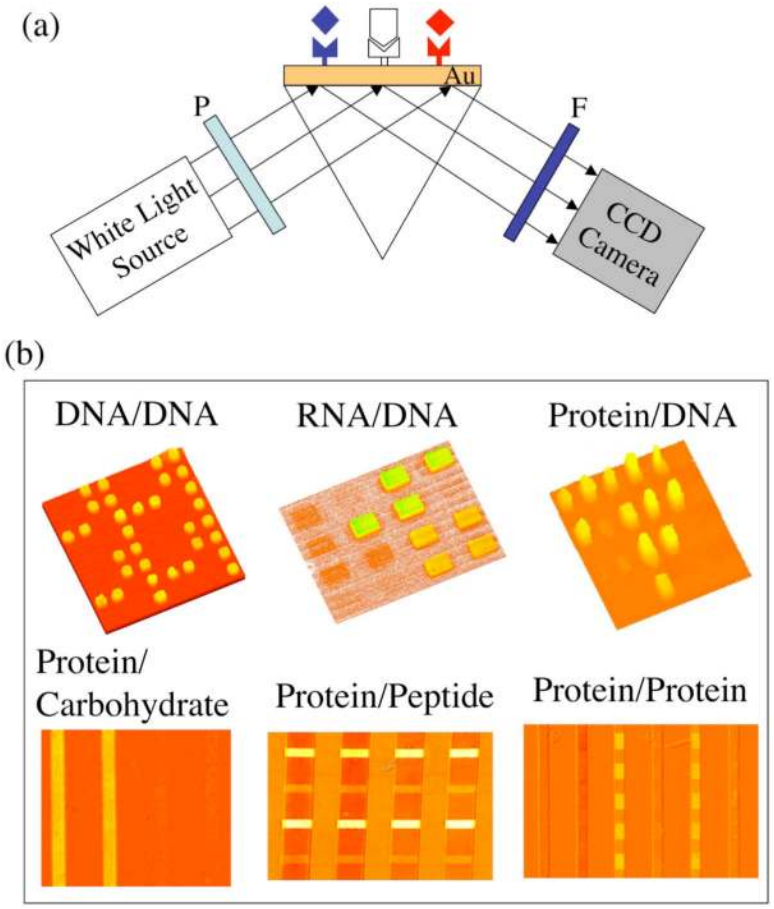

Figure 1.

(a) Schematic overview of SPRI apparatus. **P** and **F** correspond to a polarizer and an 830 nm narrow band pass filter, respectively. The output from a collimated white light source is passed through **P**, generating p-polarized light, which impinges onto a high index prism/sample assembly at an optimal incident angle. The sample is a chemically modified thin gold film that is patterned with biomolecules prior to sample assembly. Next, the reflected light is passed through **F** and focused onto a CCD camera. (b) From left to right, representative SPR difference images obtained for sequence specific 16mer ssDNA hybridization adsorption onto an ssDNA microarray, 18mer ssRNA hybridization adsorption onto an ssDNA microarray, response regulator protein binding onto a dsDNA microarray, lectin binding onto a carbohydrate line array, antibody binding onto a peptide microarray, and protein interactions with a his-tagged protein microarray.

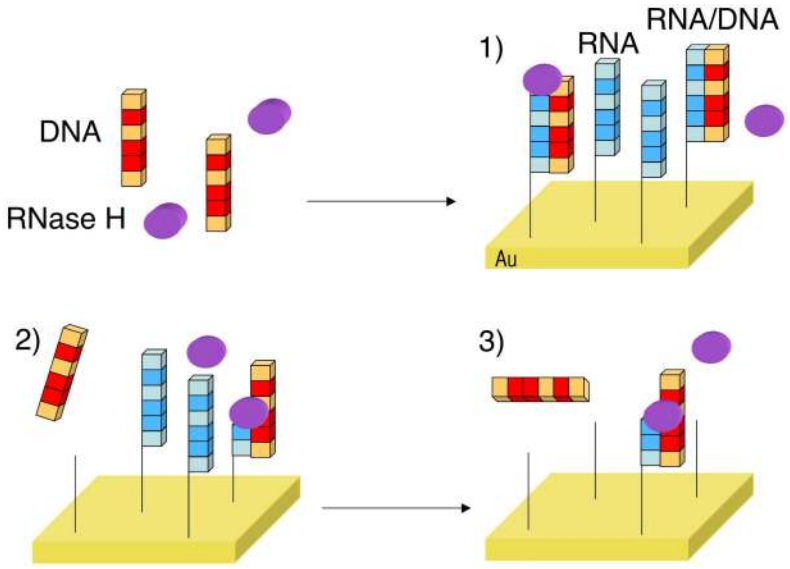

Figure 2.
Reaction scheme outlining RNase H amplified detection of target DNA using an RNA microarray. Reprinted with permission from *J. Am. Chem. Soc.* **76** 4086-4087, Copyright (2004) American Chemical Society.

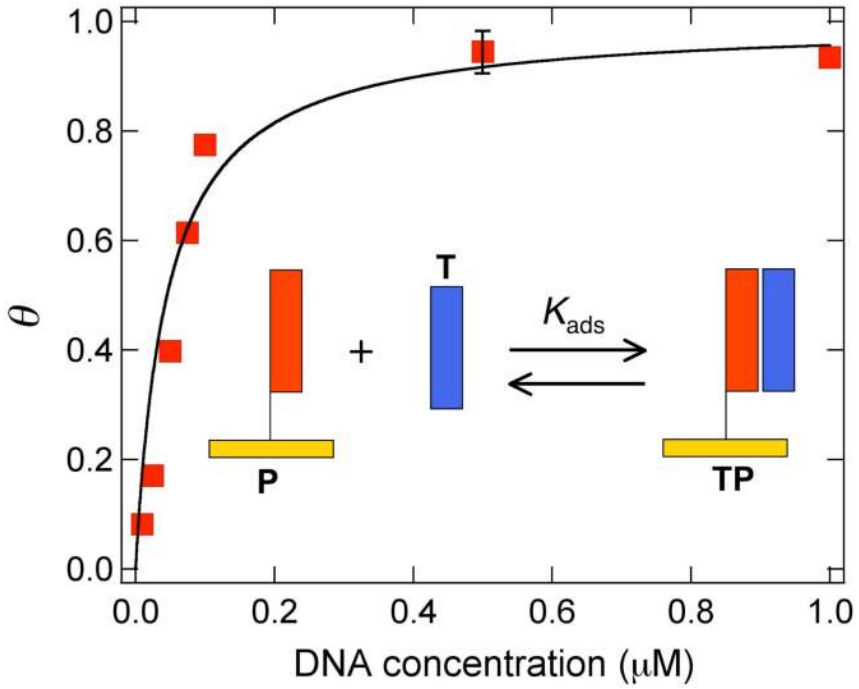

Figure 3.

Representative plot of relative surface coverage (θ) as a function of target DNA concentration. The solid line represents a Langmuir isotherm fit to the data, from which a value of $K_{ads} = 2.0 \times 10^7$ M^{-1} was determined. Inset is a schematic representing target ssDNA (**T**) hybridization adsorption onto ssDNA microarray elements (**P**).

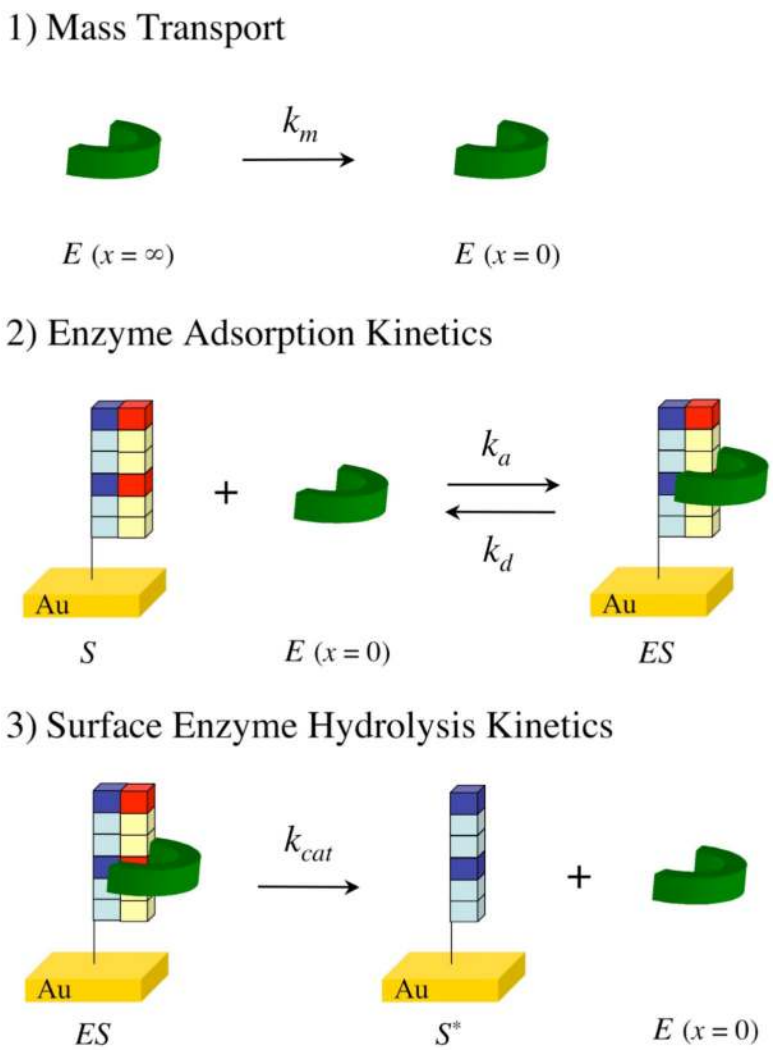

Figure 4.

Reaction scheme showing the surface enzymatic processing of a biopolymer microarray involving 1) mass transport, 2) enzyme adsorption onto a surface bound substrate, and 3) a surface enzyme hydrolysis reaction. Reprinted with permission from *Anal. Chem.* **77** 6528-6534, Copyright (2005) American Chemical Society.

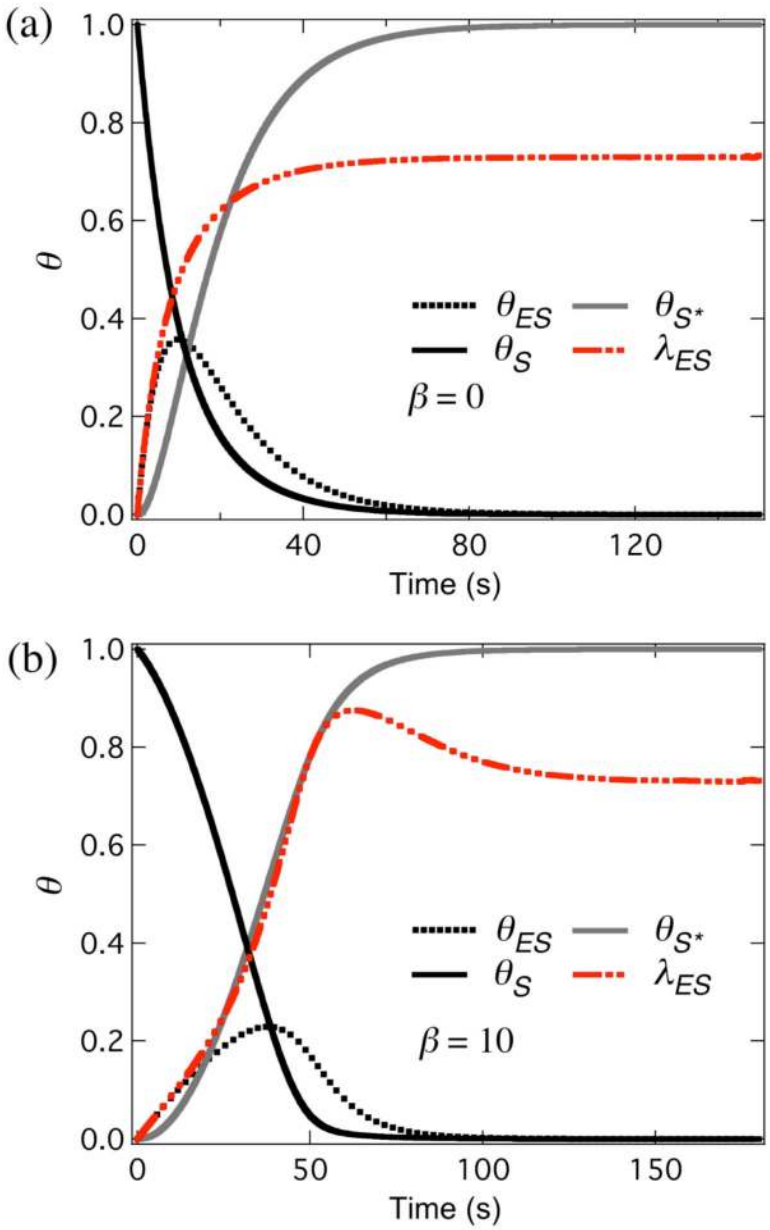

Figure 5.

Kinetic simulations of the surface enzyme reaction defined using eqs 10-12 for (a) $\beta = 0$ and (b) $\beta = 10$. All other parameters used in both (a) and (b) are identical with values of $k_a[E] = k_{cat} = 0.1\ s^{-1}$ and $k_d = 0.01\ s^{-1}$. The steady state value for λ_{ES} in both (a) and (b) is 0.728.

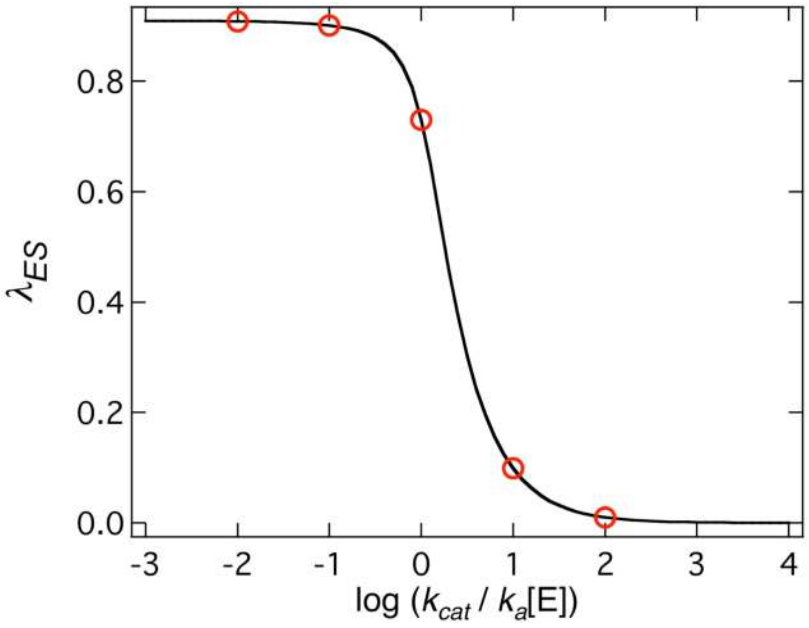

Figure 6.

Plot of the steady state value of λ_{ES} obtained using eq 15 as a function of log ($k_{cat}/k_a[E]$) with the values of $k_a[E] = 0.1\ s^{-1}$ and $k_d = 0.01\ s^{-1}$. When $k_{cat} = k_a[E]$ the value of λ_{ES} is 0.728. The λ_{ES} values of 0.901 and 0.909 are obtained when k_{cat} is respectively 10 times and 100 times smaller than $k_a[E]$. Note that the value of 0.909 is the same as θ_{eq} calculated using eq 4. When k_{cat} is 10 times and 100 times greater than $k_a[E]$, the respective values of λ_{ES} are 0.099 and 0.010.

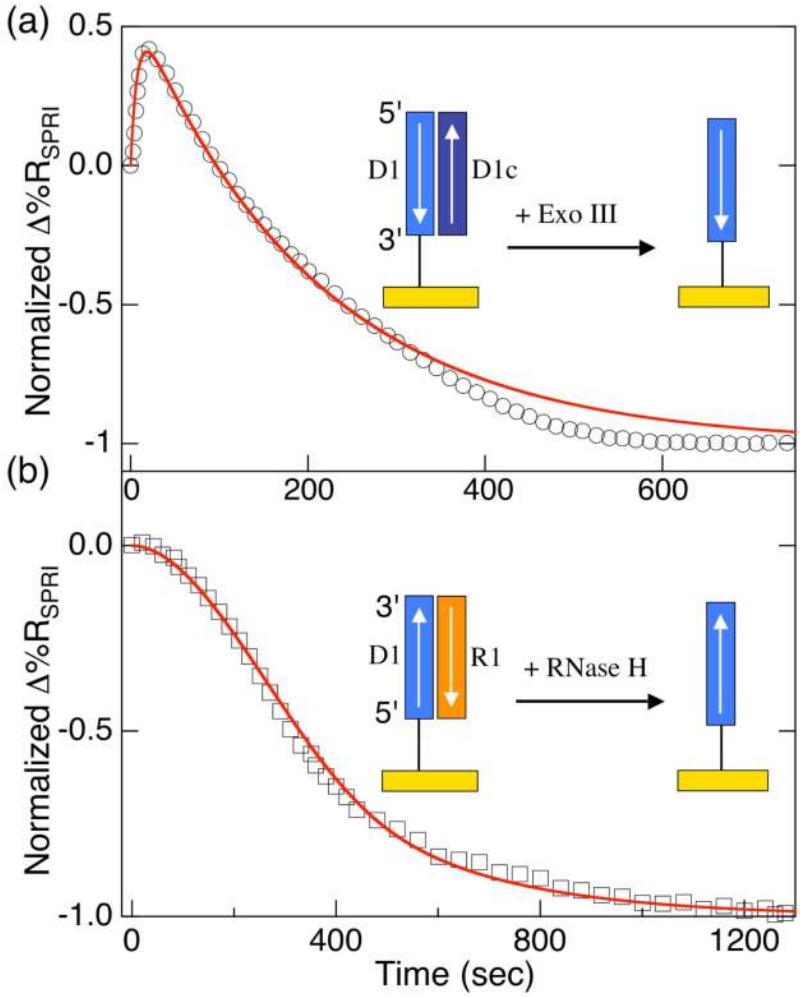

Figure 7.

Theoretical analysis of real time SPRI data measuring (a) Exo III (○) hydrolysis of a surface bound dsDNA microarray (D1-D1c) at 20°C and (b) RNase H (□) hydrolysis of a surface immobilized DNA-RNA heteroduplex (D1-R1) at 23°C. The solid lines represent model fits obtained using eqs 10-12. For RNase H, $k_a = 3.4 \times 10^6$ $M^{-1}{\cdot}s^{-1}$, $[E] = 1$ nM, $k_d = 0.1$ s^{-1}, $k_{cat} = 1.0$ s^{-1}, and $\beta = 180$ were obtained, while for Exo III, $k_a = 2.2 \times 10^5$ $M^{-1}{\cdot}s^{-1}$, $[E] = 320$ nM, $k_d = 0.056$ s^{-1}, $k_{cat} = 0.009$ s^{-1} and $\beta = 0$. The figure insets in (a) and (b) show schematic representations of the Exo III and RNase H reactions, respectively. Figure 7a reprinted with permission from *Langmuir* **21** 4050-4057 Copyright (2005) American Chemical Society.

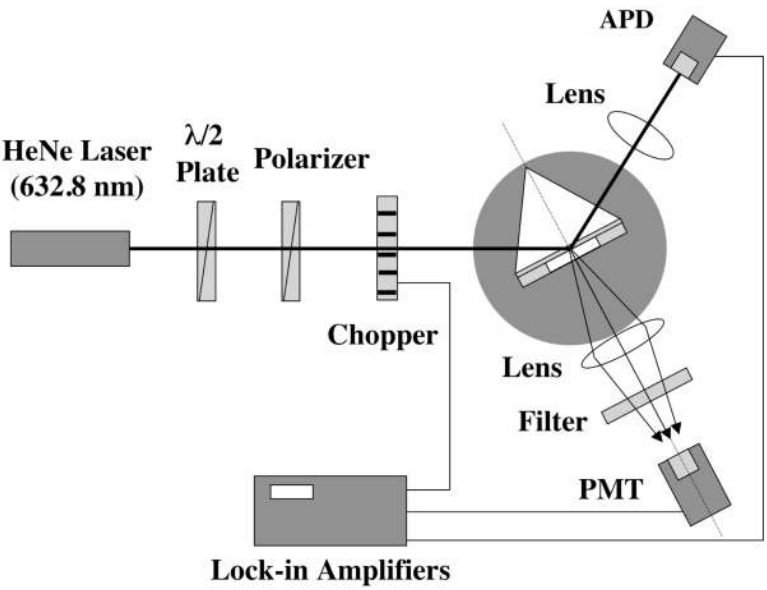

Figure 8.

Schematic illustration of setup used in SPFS-SPR measurements. The collimated beam from a HeNe laser source (λ = 632.8 nm) is passed through a λ/2 wave plate and a polarizer to attenuate the laser power to approximately 2 μW. The incident beam is modulated using a mechanical chopper with the reflected beam from the rotation stage mounted flow cell/gold film/prism assembly monitored using an avalanche photodiode detector (APD). The collected fluorescence emission from surface bound labeled molecules is focused onto a photomultiplier tube (PMT) via an interference filter. The signal output of both the PMT and APD is monitored with a lock-in amplifier. All SPFS measurements are obtained with the sample assembly positioned at a fixed optimal incident angle. Reprinted with permission from *Anal. Chem.* **77** 6528-6534 Copyright (2005) American Chemical Society.

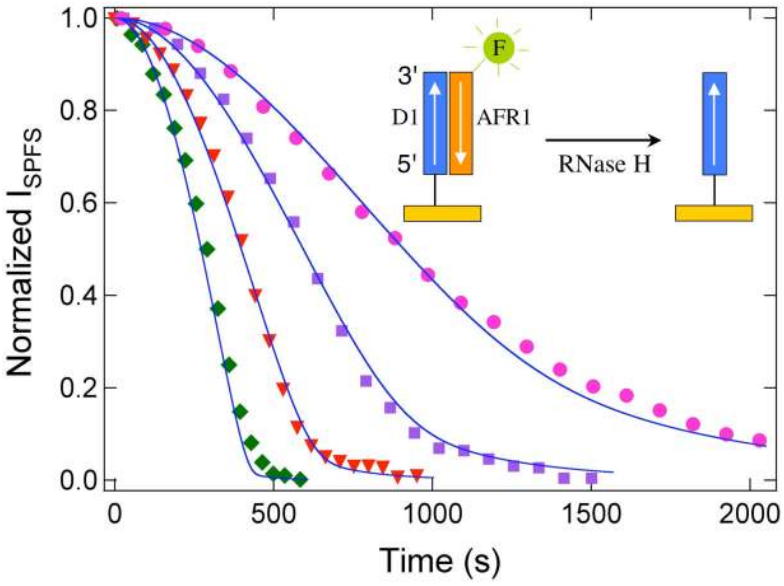

Figure 9.

Real time SPFS curves obtained for the surface RNase H hydrolysis of fluorescently labeled RNA-DNA (AFR1-D1) heteroduplexes at various RNase H concentrations (0.5 nM (●), 1.0 nM (■), 2.0 nM (▼) and 4.0 nM (◆)). The solid lines represent the simulated kinetic curves fitted using eqs 10-12 with the parameters $k_a = 2.9 \times 10^6\ M^{-1}{\cdot}s^{-1}$, $k_d = 0.10\ s^{-1}$, $k_{cat} = 0.9\ s^{-1}$ and $\beta = 650$. All SPFS signals were normalized between zero and one with the value of one corresponding to a full monolayer of AFR1-DNA heteroduplexes. Inset shows a schematic of RNase H hydrolysis of the surface-bound heteroduplex. Reprinted with permission from *Anal. Chem.* **77** 6528-6534 Copyright (2005) American Chemical Society.

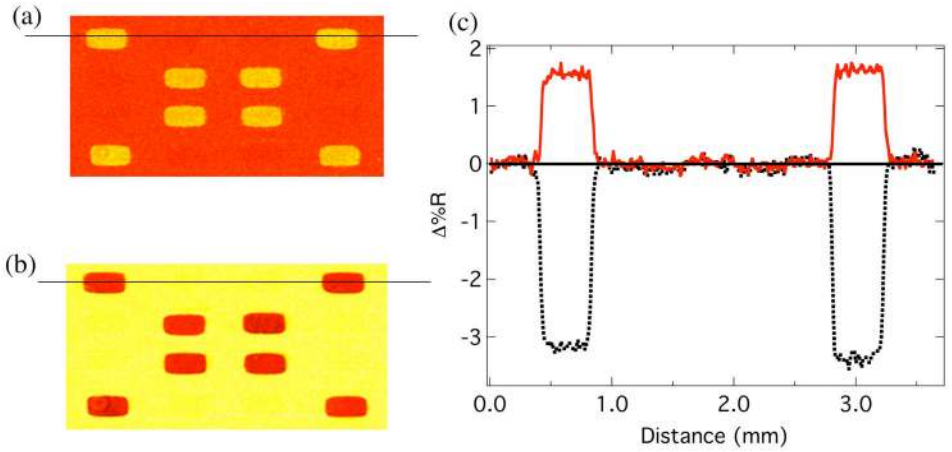

Figure 10.

SPR difference images showing (a) sequence specific hybridization of a 100 nM solution of target DNA onto ssRNA microarray elements, and (b) RNase H hydrolysis of an ssRNA array exposed to a solution containing 100 pM complementary target DNA and 8 nM RNase H for 30 minutes. (c) Comparison of line profiles in both images. The upper line profile shows an increase in percent reflectivity due to hybridization adsorption of 100 nM target DNA, while the lower line profile shows a larger decrease in percent reflectivity using a much lower concentration of target DNA (100 pM). The decrease of -3.2 Δ%R corresponds to the complete removal of ssRNA probes due to repeat cycles of hybridization adsorption of target DNA followed by RNase H hydrolysis.

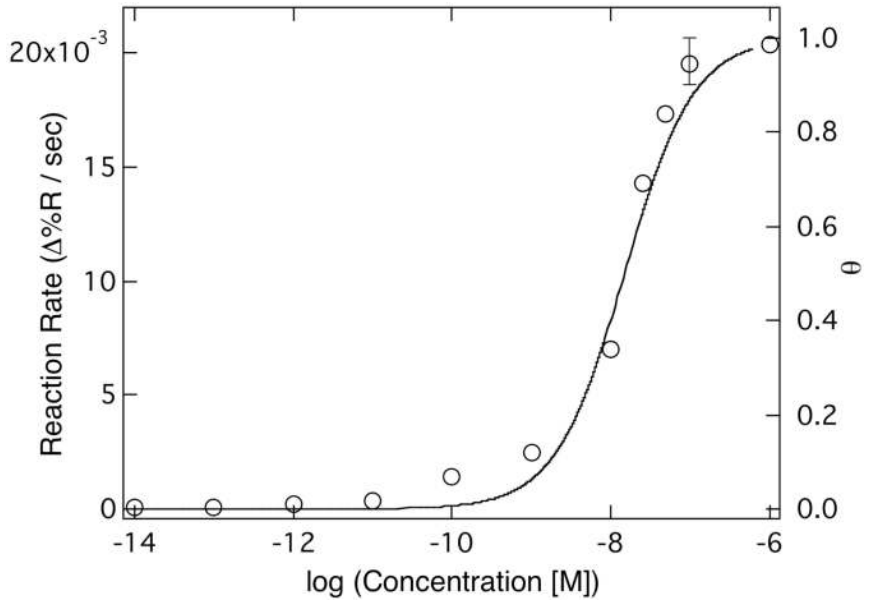

Figure 11.

A plot of initial RNase H reaction rates obtained from time dependent SPRI measurements at different target DNA concentrations. This data was normalized and fitted to a Langmuir isotherm (solid line) with a K_{ads} of 6.6×10^7 M^{-1} calculated from the fit. Reprinted with permission from *Anal. Chem.* **76** 6173-6178 Copyright (2004) American Chemical Society.

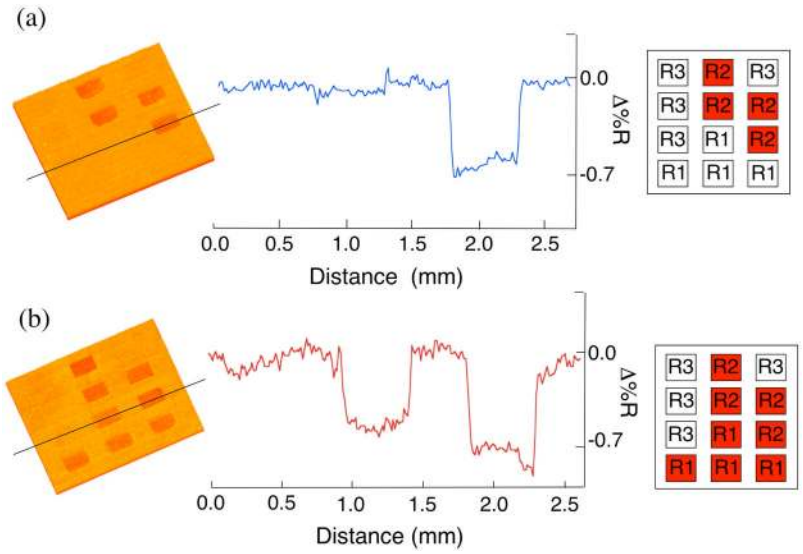

Figure 12.

(a) SPR difference image showing the RNase H amplified detection of 1 fM 20mer target DNA using an RNA microarray. The line profile taken across the difference image shows a decrease in percent reflectivity (-0.7 Δ%R) at the R2 probe elements only, with no changes in SPR signal observed at the R1 and R3 array elements. A schematic of the three-component RNA microarray is shown on the right. (b) SPR difference image obtained for the detection of 7 fM male genomic DNA using the RNase H amplification method. The line profile displays a decrease in percent reflectivity for the R1 and R2 array elements where hybridization adsorption followed by RNA probe hydrolysis occurred. The pattern of the three-component array is also shown with the RNA probes R1 and R2 designed to selectively bind to the TSPY gene on the Y chromosome and R3 used as a negative control. Reprinted with permission from *J. Am. Chem. Soc.* **126** 4086-4087 Copyright (2004) American Chemical Society.

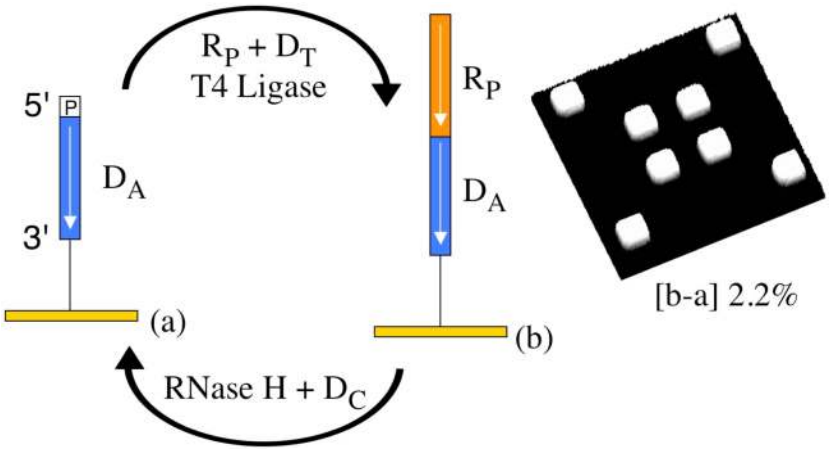

Figure 13.

Simplified schematic for the fabrication of a renewable ssRNA microarray via RNA-DNA ligation chemistry and RNase H hydrolysis. The ssRNA microarray was created by the selective ligation of R_P onto the D_A elements of a two-component DNA microarray. Hybridization of complementary DNA (D_C) onto the ligated ssRNA followed by the selective hydrolysis of RNA using RNase H regenerates the original 5′ phosphorylated ssDNA surface. A representative in-situ SPR difference image [b - a] obtained by subtracting images acquired before hybridization/ligation and after removal of DNA template (D_T) from the array surface. Reprinted with permission from *Anal. Chem*. **77** 7832-7837, Copyright (2005) American Chemical Society.

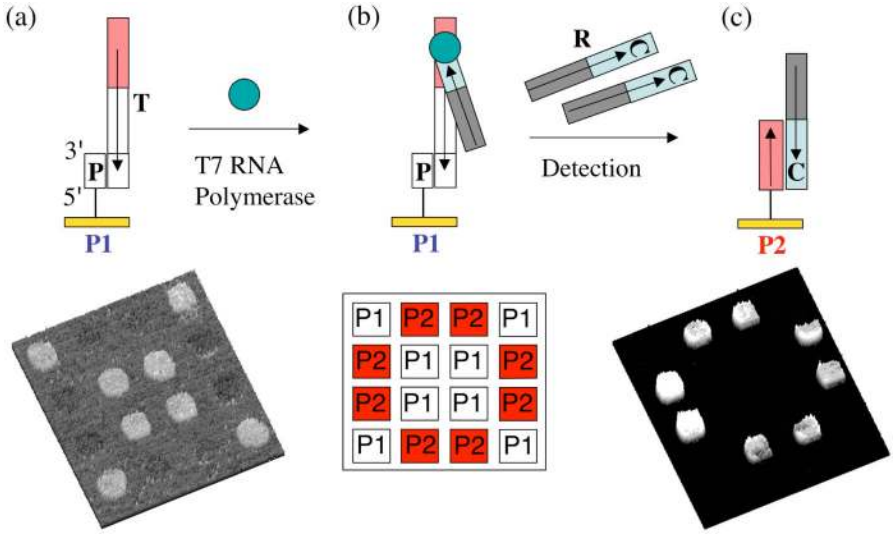

Figure 14.

Schematic describing the replication of ssRNA from a dsDNA microarray element (P1) using T7 RNA polymerase and the subsequent detection of the replicated ssRNA molecules via hybridization adsorption onto a second array element (P2). (a) Hybridization adsorption of complementary template DNA (T) at P1 elements. The double stranded promoter region (P) is recognized by T7 RNA polymerase. (b) Replication of multiple ssRNA (R) copies. (c) Detection of R via hybridization at the P2 elements with the color scheme indicating complementary regions between the ssRNA and P2 ssDNA sequences. The left side SPR difference image measures the hybridization adsorption of complementary template DNA (T) onto P1 array elements. This microarray is then exposed to T7 RNA polymerase with the right side SPR difference image demonstrating the detection of transcribed ssRNA at the P2 array elements. Note that for this preliminary SPRI data, the length of the surface attached ssDNA on the P1 elements is the same length as the T sequence (85 bases). The P promoter region (which is 37 bases long) is double stranded. The ssDNA sequence attached onto the P2 array elements is a 20mer. The ssDNA used in both the P1 and P2 elements are thiol-modified at the 5′-end allowing surface immobilization via maleimide linking chemistry. The ssRNA sequence synthesized via T7 RNA polymerase is 63 bases long.

Table 1

Summary of kinetic model parameter values obtained using eqs 10-12 and 15 to fit SPRI and SPFS data sets for the surface hydrolysis reactions of Exo III[38] and RNase H.[44]

Kinetic parameters (units)	Exo III (SPRI)	RNase H (SPRI)	RNase H (SPFS)
k_a ($M^{-1}\cdot s^{-1}$)	2.2×10^5	3.4×10^6	2.9×10^6
k_d (s^{-1})	0.056	0.1	0.1
k_{cat} (s^{-1})	0.009	1.0	0.9
λ_{ES}	0.54	3.1×10^{-3}	2.9×10^{-3}
θ_{eq}	0.56	0.033	0.028
β	0	180	650